Zhen Chen ✉
Chaocheng Wei
Shulong Nie
Ling Liu
Shuang Jing
Zhiqiang Huang
Lei Hao
Guangjing Zhou

https://doi.org/10.21278/TOF.483058123
ISSN 1333-1124
eISSN 1849-1391

THE VIBROSEIS BASEPLATE VIBRATION DAMAGE FAILURE MECHANISM AND THE PREDICTION OF FATIGUE LIFE

Summary

The present study investigates the impact of earthquake excitation on vibroseis, which can lead to fatigue failure and cracking of the welded area of a baseplate. This reduction in service life adversely affects the quality of geophysical prospecting signals. To mitigate this issue, the study develops a vibrator-geodetic coupling model. It investigates the calculation method and loading law for generating baseplate output force, uncovering the underlying damage mechanisms through macroscopic and micro-morphological analysis. Fatigue tests using a three-point bending method establish correlations with the observed characteristics. The method of fitting S-N curves and the model for predicting lifespan significantly improve the accuracy and efficiency of predicting the baseplate lifespan. The findings support the enhancement of reliability in vibrators and baseplates, with potential applications in the research and development of oil and gas exploration technology and engineering equipment.

Key words: *vibroseis baseplate; vibration mechanics; damage mechanisms; three-point bending fatigue test; fatigue life*

1. Introduction

Vibroseis is a highly efficient, green, safe, and inexpensive geophysical exploration technology and is considered a ‘sharp weapon’ in the field of oil and gas exploration. However, a welded vibroseis baseplate not only suffers a huge load from the vibroseis truck but is also repeatedly subjected to high and wide frequency vibrations from the vibrator. Such harsh working conditions can cause fatigue and fracture failure in the welded part of the baseplate, as shown in Fig. 1. In addition, the strength and fatigue resistance of a defective vibrator baseplate is highly complex and random due to the continuous high and low frequency shocks. As a result, this type of fracture always occurs unexpectedly and is very difficult to accurately predict. At present, the best methods to address fatigue fracture are replacing parts and welding repairs. The total number of A type vibroseis trucks in service internationally is as high as 34. According to statistical data

in the field, cracking phenomena exist in 27 vibrator baseplates, accounting for 79 percent of the total number. Most cracks have an obvious influence on the construction quality of the baseplate and necessitate its replacement. Such a sudden development of the fracture greatly reduces the geophysical construction efficiency. Therefore, the early and accurate prediction of baseplate fatigue life can provide valuable guidance for the use of reinforcement measures, which will effectively prevent the baseplate's sudden fracture and prolong its service life.

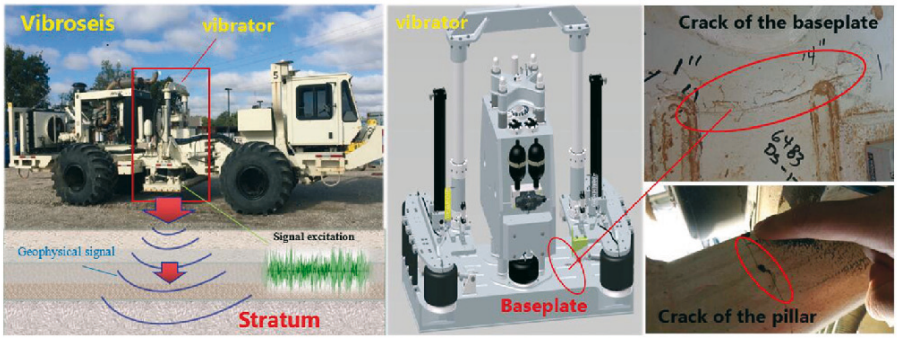

Fig. 1 Cracks present on the baseplate surface and pillar

Several studies have been reported in the literature related to the prediction of fatigue life, and two methods are widely used to predict it. (1) The first is the cumulative damage method (S-N curve method). Gao Zhentong [1] developed a theoretical formula for determining the distribution function of fatigue strength using the *P-Sa-Sm-N* surface. Additionally, Keceeiogfu [2] used the residual strength life model and cumulative damage model to calculate the reliability life of structures subjected to different cyclic stress levels. These research results provided an important early basis for the prediction of fatigue life. Kan Ni [3] developed fatigue reliability with the two-dimensional probabilistic Miner criterion which suffered from the random time load. Zhixiao Su [4] carried out a two-dimensional distribution of stress cycles characteristic analysis with the one-dimensional distribution method, where the fatigue life and reliability calculation method were both used. The distribution characteristics of stress and the S-N curve were considered in the life prediction and reliability analysis. Gu Yi [5] discussed the critical damage and transient cumulative damage characteristics based on the damage definition. In 2011, Qinhua Wang [6] developed a wind source fatigue reliability analysis, where the results showed that the random variables of the *S-N* curve had a great effect on the failure probability of the failure model. The *S-N* curve method is a very common and effective fatigue life and fatigue reliability theory. However, it is highly dependent on the materials fatigue test for the real *S-N* curve to obtain accurate reliability results. (2) The other popular method is the fracture mechanics method (crack propagation method) based on the Paris [7] and Forman formulas for the fatigue cycle from crack initiation to structural failure. In 1920, A.A. Griffith [8] developed theoretical and experimental research of the glass brittle fracture, and proposed an energy theory of crack propagation, which is the foundation of fracture mechanics. J.A. Bea [9] presented a new model of predicting the fatigue crack propagation life of metal structural components. In this new model, he took the initial and final crack length, the crack propagation angle, fracture parameters, elastic parameters, and external load as random variables. In 2014, Chaoyang Shi [10] adopted the fracture mechanics theory and established the residual fatigue life assessment model of a bridge crane metal structure under constant amplitude loading, considering the effect of the stress ratio. In 2010, Xueyin Wang [11] studied the fatigue life prediction of a welded ball node grid structure based on the fracture mechanics theory. He deduced two theoretical fatigue life prediction formulas, using the Paris and Forman crack growth rate formula, respectively. In 2016, B. Alfredsson [12] conducted research on physically short cracks propagating in bainitic high-strength bearing steel, under the fatigue load. As mentioned above, predicting fatigue life by the fracture mechanics method reflects the

loading cycles from the initial crack length to the final fracture. This is an effective way to obtain the structure of fatigue life and is much closer to engineering reality. However, it has higher statistical requirements for the microscopic parameters of the baseplate structure (initial crack, the critical crack size, and so on), and the calculation accuracy of the fatigue reliability of this method is difficult to control.

Meanwhile, the baseplate damage failure mechanism has not yet been revealed, but it provides important theoretical support for the analysis of baseplate fatigue behaviour and anti-fatigue optimisation. Researchers worldwide have mainly adopted the fatigue test method and cumulative damage theory to analyse the fatigue damage mechanism. Gu Yi [5] used the Miner damage theory to study the fatigue cumulative damage models associated with structural elements and discussed critical damage and instantaneous damage characteristics. Cumulative damage was described as a random process, and a mathematical expression was determined. Tan Xiaoming [13] analysed the fatigue fracture surface of an aluminium alloy sheet using scanning electron microscopy (SEM) and revealed the fatigue damage rule for an aluminium alloy plate subjected to complex loads.

Above all, research has mainly focused on the fatigue life analysis of conventional mechanical structures by using the methods of the S-N curve and fracture mechanics. Few studies have been reported on the fatigue life of vibroseis baseplates. Besides, the coupling vibration of the mechanical behaviour and the internal damage mechanism are unclear. It is very difficult to predict the baseplate fatigue life due to the significant uncertainties associated with vibrator excitation. All of this results in great challenges for fatigue resistant design. In the present work, based on the baseplate structure design and welding process, a coupling vibration analysis of the vibrator-earth mechanical system was carried out. A macroscopic and microscopic morphology analysis was conducted to reveal the fatigue damage mechanism of the baseplate under alternating excitation. In addition, the advanced S-N curve method was developed to predict the baseplate service life, which greatly improved the accuracy and efficiency of the prediction. The results will enhance the fatigue resistant performance of the baseplate, reduce the probability of fatigue failure, and prevent the baseplate from experiencing a sudden fracture.

2. Review of the vibrator baseplate design

The vibrator is the key component of vibroseis and is used to excite the seismic signal. To obtain a higher-quality signal, the structure and performance of the vibrator has undergone several changes, and there are many vibrator baseplate structures. In 1978, Western Geophysical, an American company, proposed a rectangular baseplate composed of I-beam (as shown in Fig. 2) or T-shaped steel [14]. INOVA, another American company, designed a rectangular baseplate using square steel beams. In 2010, in an attempt to solve the problems of poor rigidity, uneven forces and large deformations in the I-beam steel baseplate, a new skeleton baseplate was introduced by the Bei Ao special vehicle company (Fig. 3). In 2012, INOVA developed a new baseplate composed of a carbon fibre composite non-metallic baseplate (Fig. 4).

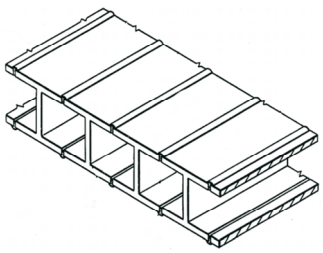

Fig. 2 I-beam welded baseplate

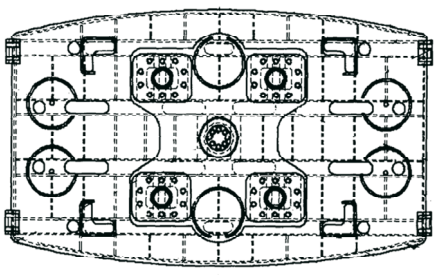

Fig. 3 New skeleton baseplate

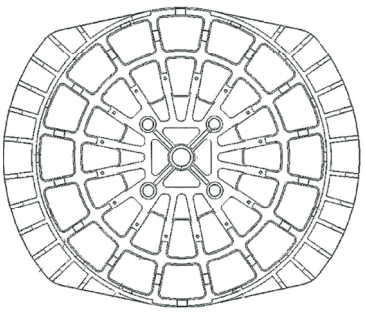

Fig. 4 Composite non-metallic baseplate

Presently, due to the high quality, rigidity, and signal precision requirements of the baseplate, as well as the manufacturing cost, the I-beam and rectangular tube versions are the most commonly used vibroseis baseplates (Fig. 5). The entire baseplate is group welded side by side with the rectangular tubes. A mixed steel skeleton structure is applied to support the bottom of the baseplate and is welded to the adjacent rectangular tube. Rectangular plates are arranged along the length direction of the baseplate to increase the global stiffness [15].

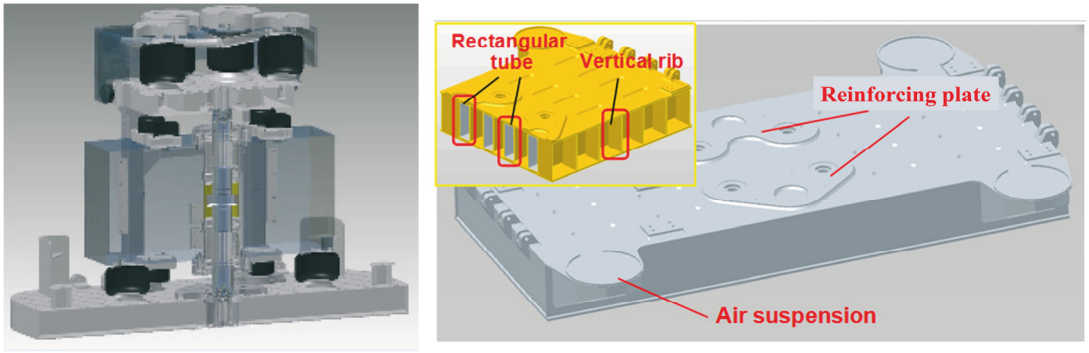

Fig. 5 Structure of the vibrator and baseplate

Vibroseis baseplates are most often welded. According to the baseplate design concept, to improve the excitation energy transfer rate, to decrease the decoupling rate, and to improve the stress distribution of the baseplate, the baseplate design focuses on enhancing the stiffness and ignores the welded structure's fatigue resistance.

3. Analysis of the vibrator dynamic mechanism response

The analysis of the characteristics of the vibrator baseplate dynamic response usually uses the weighted sum method proposed by Sallas [16]. This method assumes that the baseplate is a rigid body and that it completely couples to the earth. In this case, the output force is the vector sum of the hammer and baseplate. However, an absolutely rigid baseplate cannot actually be produced, and complete coupling between the baseplate and the earth does not exist. In addition, the coupling adhesion effect of the soil and the baseplate is always neglected. All these factors reduce the calculation accuracy of the weighted sum method. In this paper, the elastic half space theory is applied based on the Sallas model and considers the soil adhered to the baseplate as part of the vibrator [17]. Then, the vibrator can be assumed to act as a mass spring damping system.

3.1 Hypotheses

Due to the complex characteristics and closeness to the earth, it is very difficult to analyse the stress-strain and output force of the baseplate subjected to a cyclical force. Therefore, the idealised soil model is chosen according to the soil characteristics and the external load [18-28]. The hypotheses used here are as follows:

(1) The near surface soil is chosen as an elastic continuum model, and the soil medium is regarded as an ideal three-dimensional continuous elastic body.

(2) Under the external load, the distributions of the soil displacement, stress and strain are continuous.

3.2 Determination of parameters

According to the elasticity theory, the elastic and damping coefficient of the near surface soil medium can be calculated from [28]

$$G_v = \frac{1}{2}\sqrt{\rho G_s S \sqrt{S}} \tag{1}$$

where s ρ is the soil density of 1750 kg/m^3, S is the baseplate area of 2.49 m^2, E is the modulus of elasticity of the soil of 5×10^7 Pa, and v is Poisson's ratio of 0.4. According to Eqs. (1) and (2), the coefficient of elasticity of the soil medium is G_s=1.061×10^8, and the earth damping coefficient is G_v=4.2714×10^5. The vibrator parameters are shown in Table 1.

Table 1 Vibrator parameters

Hammer mass *Mr* (kg)	Baseplate mass *Mb* (kg)	Hydraulic oil elastic coefficient k_1	Spring coefficient of air spring k_2
3683	1823	5.15×10^5	1.1×10^5
		Hydraulic oil damping coefficient C_1	Air spring damping coefficient C_2
		1.5×10^3	8.5×10^3

3.3 Model establishment

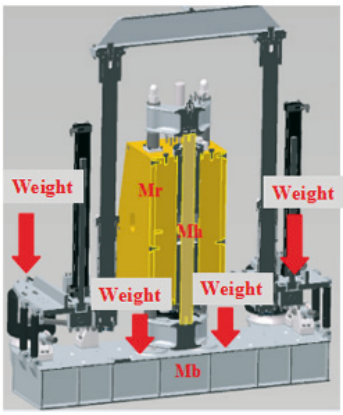

Fig. 6 3-D model of the vibrator structure

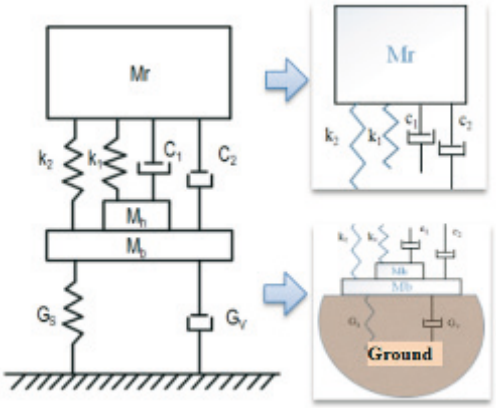

Fig. 7 Vibration system model

In the vibrator system model, we assume that the hammer vibrates only in the vertical direction, the vibration axis is symmetrical and coincides with the centre line of the piston rod, and there is no torsion movement (Fig. 6). The dynamic model of the vibrator is shown in Fig. 7.

Under the exciting load, the displacement of the piston rod and hammer are X_r and the displacement of the baseplate is X_b. The kinematic equations are given by:

$$M_r\ddot{X}_r + (k_1+k_2)(X_b - X_r) + (C_1+C_2)(\dot{X}_b - \dot{X}_r) = F_m \sin\omega t \tag{2}$$

$$(M_h+M_b)\ddot{X}_b + G_sX_b + G_v\dot{X}_b - (k_1+k_2)(X_b - X_r) - (C_1+C_2)(\dot{X}_b - \dot{X}_r) = F_m \sin\omega t \tag{3}$$

3.4 Model solution

The vibration is dominated by a steady state process. The special solutions are:

$$X_r = A_1 \sin\omega t + A_2 \cos\omega t$$

$$X_b = B_1 \sin\omega t + B_2 \cos\omega t$$

Substituting X_r, $\dot{X}_r$, $\ddot{X}_r$ and X_b, $\dot{X}_b$, $\ddot{X}_b$ into equations (3) and (4) results in simplified versions of the equations:

$$-(M_r\omega^2 + k_{12})A_1 + k_{12}B_1 + C_{12}\omega A_2 - C_{12}\omega B_1 = F_m \tag{4}$$

$$-C_{12}\omega A_1 + C_{12}\omega B_1 - (M_r\omega^2 + k_{12})A_2 + k_{12}B_2 = 0 \tag{5}$$

$$k_{12}A_1 + (G_s - k_{12} - M_{hb}\omega^2)B_1 - C_{12}\omega A_2 + (C_{12} - G_v)\omega B_2 = F_m \tag{6}$$

$$C_{12}\omega A_1 + (G_v - C_{12})\omega B_1 + k_{12}A_2 + (G_s - k_{12} - M_{hb}\omega^2)B_2 = 0 \tag{7}$$

Solving equations (5), (6), (7) and (8), we arrive at:

$$B_1 = \frac{k_{12}d - C_{12}\omega b}{bc - ad} \cdot F_m \tag{8}$$

$$B_2 = \frac{C_{12}\omega a - k_{12}c}{bc - ad} \cdot F_m \tag{9}$$

$$A_1 = \frac{(G_s - M_{hb}\omega^2)B_1 - G_v\omega B_2 - F_m}{M_r\omega^2} \tag{10}$$

$$A_2 = \frac{G_v\omega B_1 + (G_s - M_{hb}\omega^2)B_2}{M_r\omega^2} \tag{11}$$

where

$$k_{12} = k_1 + k_2$$

$$C_{12} = C_1 + C_2$$

$$a = k_{12}M_r\omega^2 - (M_r\omega^2 + k_{12})(G_s - M_{hb}\omega^2) + C_{12}G_v\omega^2$$

$$b = (M_r\omega^2 + k_{12})G_v\omega - C_{12}M_r\omega^3 + C_{12}(G_s - M_{hb}\omega^2)\omega$$

$$c = M_r\omega^3 C_{12} - C_{12}\omega(G_s - M_{hb}\omega^2) - (M_r\omega^2 + k_{12})G_v\omega$$

$$d = C_{12}G_v\omega^2 - (M_r\omega^2 + k_{12})(G_s - M_{hb}\omega^2) + k_{12}M_r\omega^2$$

Substituting equations (9), (10), (11), and (12) into X_r and X_b results in:

$$X_{\mathrm{r}} = x_r\cos(\omega t + \alpha_1)$$

$$X_b = x_b\cos(\omega t + \alpha_2)$$

$$x_r = \sqrt{A_1^2 + A_2^2} \tag{12}$$

$$x_b = \sqrt{B_1^2 + B_2^2} \tag{13}$$

3.5 Model solution

For the vibrator, the force transmitted from the baseplate to the earth is the vibrator output force, which is equal to the sum of the spring and damping forces caused by the relative motion of the vibrator baseplate:

$$F_d = G_s X_b + G_v\dot{X}_b \tag{14}$$

$$F_d = G_s x_b\cos(\omega t + \alpha_2) - G_v\omega x_b\sin(\omega t + \alpha_2) \tag{15}$$

At the initial phase α_2=0°:

$$F_d = G_s x_b\cos(\omega t) - G_v\omega x_b\sin(\omega t) = J_1\sin(\omega t) + J_2\cos(\omega t) \tag{16}$$

where

$$J_1 = -30\pi G_v x_b \tag{17}$$

$$J_2 = G_s x_b \tag{18}$$

By applying the auxiliary angle formula, the simplified equation is given by:

$$F_d = \sqrt{J_1^2 + J_2^2} \cdot \sin(\omega t + \varphi) \tag{19}$$

$$\tan\varphi = \frac{J_2}{J_1} \tag{20}$$

Therefore, the maximum force is given by:

$$|F_d| = \sqrt{J_1^2 + J_2^2} = \sqrt{B_1^2 + B_2^2} \cdot \sqrt{G_s^{\,2} + (G_v\omega)^2} \tag{21}$$

$$|F_d| = x_b \cdot \sqrt{G_s^2 + G_v^2 \cdot \omega^2} \tag{22}$$

where $x_b = \sqrt{B_1^2 + B_2^2}$ is the baseplate displacement amplitude, G_s=1.061×10^8, G_v=4.2714×10^5, the frequency of the vibrator hydraulic force is f=15 Hz, and the angular frequency is ω=30π rad/s. The calculation results show that the peak output force of the vibrator baseplate is approximately 275 kN. The reaction force of the earth on the baseplate is also 275 kN. The relationship between the baseplate output force and time, the displacement, and the vibration frequency are shown in Figs. 8 and 9.

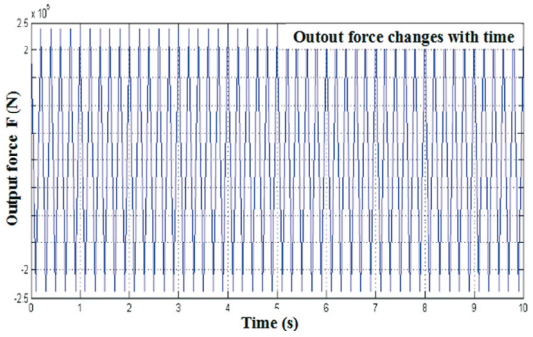

Fig. 8 The relationship between the baseplate output force and time

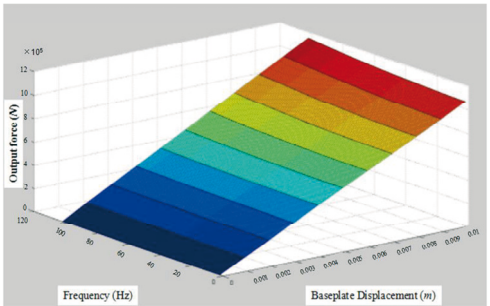

Fig. 9 The baseplate force changes as a function of frequency and displacement

The analysis results of the baseplate output force during the signal excitation show that:

(1) The loading from the earth to the baseplate changes periodically with time and reaches as much as 275 kN, which is quite large for the baseplate. As a result, components in the joint between the baseplate and piston rod are placed into a high stress state. This is an area of weakness that is susceptible to fatigue failure and high levels of deformation and damage (Figs. 10 and 11).

The analysis results of the baseplate output force during the signal excitation show that:

(1) The loading from the earth to the baseplate changes periodically with time and reaches as much as 275 kN, which is quite large for the baseplate. As a result, components in the joint between the baseplate and piston rod are placed into a high stress state. This is an area of weakness that is susceptible to fatigue failure and high levels of deformation and damage (Figs. 10 and 11).

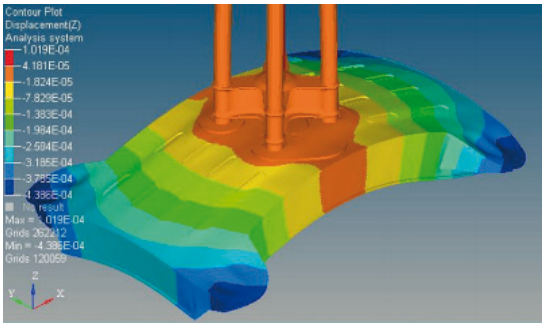

Fig. 10 Deformation of the baseplate

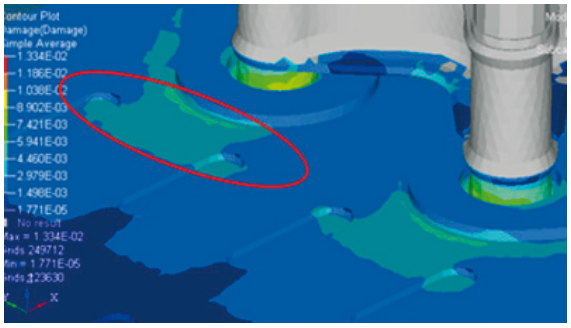

Fig. 11 Damage of the baseplate

(2) The baseplate output force increases with the vibration displacement and frequency. The broadband excitation characteristics of the vibrator lead to larger uncertainty in the baseplate output force. All these factors enhance the randomness of crack initiation, expansion rate, and time of fracture.

4. Analysis of the damage failure mechanism for the baseplate fracture

Through the micro-structure testing of the baseplate cracking position, we performed morphological analysis and fracture feature recognition at different fracture positions (weld toe fracture and substrate fracture) from damage formed as a result of certain cyclic loading. Then, the crack initiation site and crack propagation direction were determined, and routing and terminal crack morphology microscopic analysis was carried out. Finally, the fracture damage characteristics, crack propagation law, and the baseplate damage mechanism were revealed.

4.1 Testing equipment

The materials and equipment used for the baseplate fracture micro-morphology testing include: baseplate crack fracture specimens, a wire cutting machine, a PX50M type optical microscope (Fig. 12), an FEI Quanta 450 scanning electron microscope (Fig. 13), alcohol, tweezers, beakers, etc.

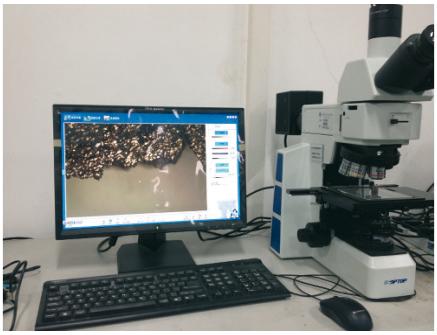

Fig. 12 PX50M metallurgical microscope

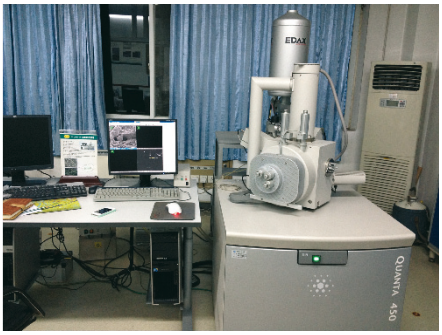

Fig. 13 Environmental scanning electron microscope

4.2 Test procedure

(1) The scrap vibrator baseplate cracked parts and fracture specimens were collected, and oxidation resistance and rust prevention treatments were developed and applied.

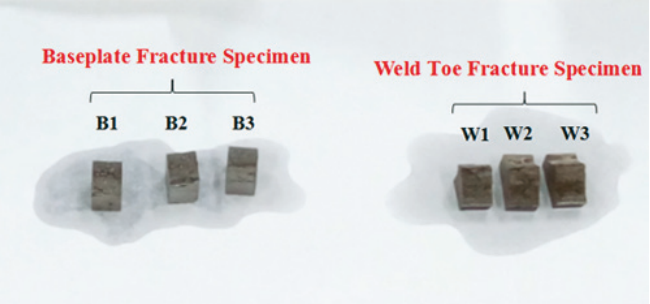

Fig. 14 Numbering the specimens

(2) The typical fracture parts (weld toe fracture and fracture cutting substrate) were cut into appropriate sizes for analysis using a wire cutting machine. Three specimens were obtained from the weld toe and substrate fractures. The surface oil and cutting fluid on the specimens were cleaned using alcohol. Then, the specimens were quickly dried and numbered. The three weld toe fracture specimens were numbered W1, W2, and W3. The substrate specimens were numbered B1, B2, and B3 (Fig. 14).

(3) At first, a low magnification PX50M metallographic microscope was used to observe the specimen fracture, and the outline and location of the crack propagation traces were determined.

(4) The microstructure of the crack initiation region, crack propagation region, and fracture failure region of the specimens were analysed using a high-speed FEI Quanta 450 scanning electron microscope [29-31].

4.3 Experimental analysis of the baseplate fatigue damage mechanism

The fatigue failure theory for metals and the micro fracture analysis of the vibrator baseplate state that the microscopic process of baseplate fatigue failure is a very complicated process that is divided into three phases: crack initiation, crack propagation, and fracture.

(1) Fatigue crack initiation mechanism for the baseplate

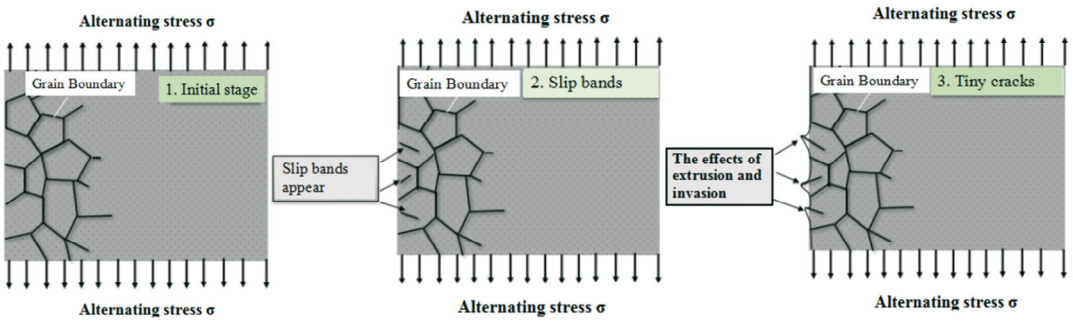

Fig. 15 Fatigue crack initiation process

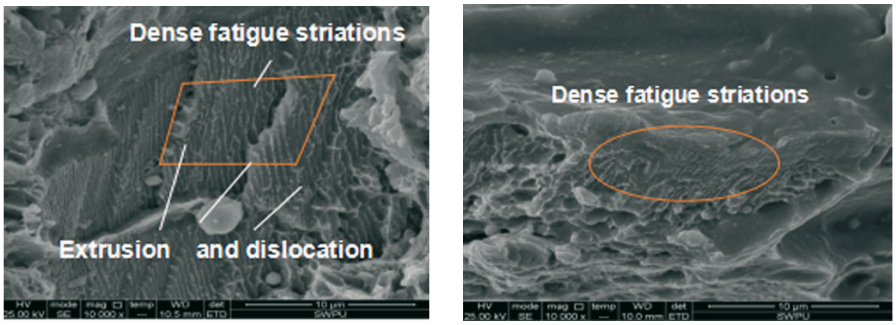

Fig. 16 Microscopic process of fatigue crack initiation in the baseplate

The fatigue cracks always originate from weld defects, including welding slag, damage, and other stress concentration sources which cannot be avoided during baseplate manufacturing and heat treatment. When operated, the baseplate is subjected to a number of stress cycles, causing some small slip lines to appear in the internal grains of the microstructure. As the number of stress cycles increases, new slip lines are generated, and wide slip bands appear. Then, tiny fatigue cracks occur among these wide slip bands. The effects of the extrusion and invasion of the wide slip bands produce many voids and more tiny cracks. The tiny cracks gradually coalesce and an initial crack is formed in this region. The process is shown in Figs. 15 and 16.

(2) The fatigue crack propagation mechanism

Once the fatigue cracks appear near the surface of the baseplate, the tiny cracks grow trans-granularly along a direction of approximately 45 degrees when subjected to a uniaxial load. With the continuous action of the cyclic load, the tiny cracks continue to expand or coalesce to form a large-scale main crack. As the growth direction becomes perpendicular to the loading plane and the growth rate increases, the contours of the stripes become clearer. The process is shown in Figs. 17 and 18.

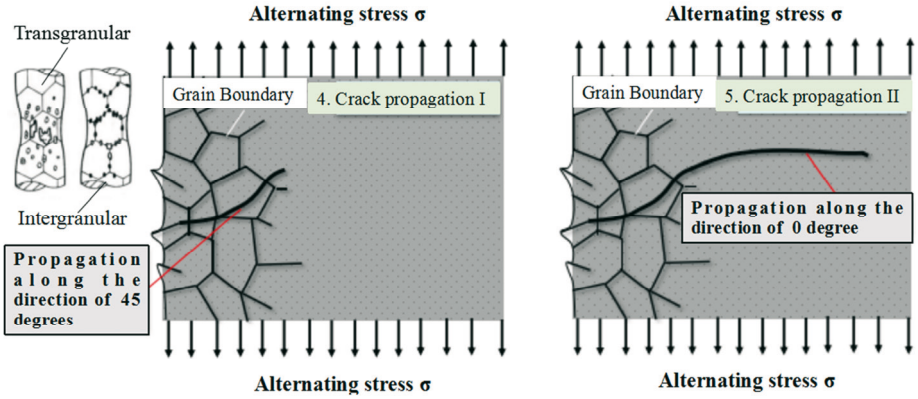

Fig. 17 Two stages of fatigue crack propagation

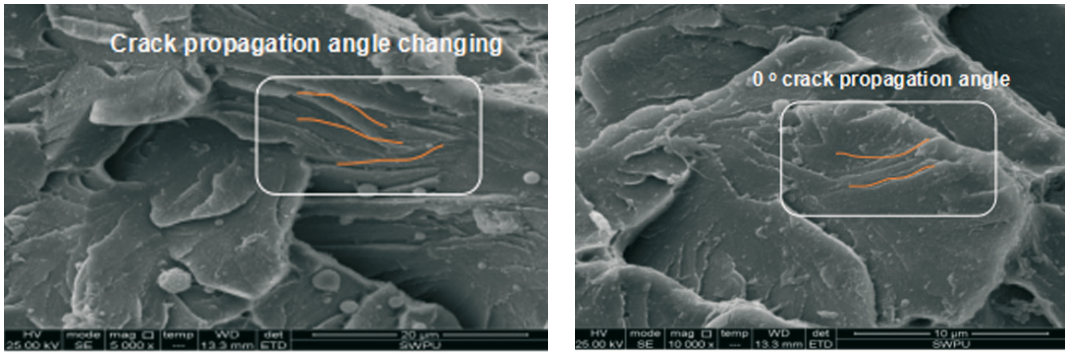

Fig. 18 Microscopic process of fatigue crack propagation within the baseplate

(3) Fracture failure stage

As the fatigue crack extends to a certain critical length, the effective section of the baseplate is gradually reduced. This slowly increases the stress in the baseplate, and the fatigue portion gradually enters the plastic deformation stage where dimple and tearing features become obvious on the crack face, as shown in Fig. 19. When the stress exceeds the material's ultimate strength, the baseplate structure rapidly fractures. This is the final stage of the baseplate's service life.

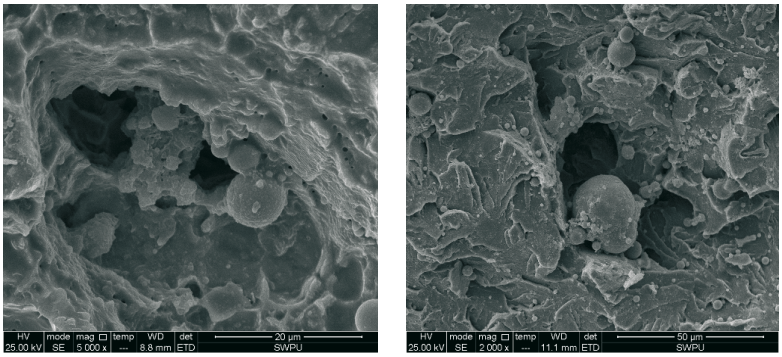

Fig. 19 Microstructure of the specimen crack face during fracture

In summary, the damage mechanisms affecting a baseplate subjected to vibration conditions can be described in three stages: fatigue crack initiation (Stage I), fatigue crack propagation (Stage II), and fracture failure (Stage III). During the first stage, tiny fatigue cracks originate from weld defects and among wide slip bands when the baseplate is subjected to an alternating load. This process forms the initial cracks. In the second stage, the tiny cracks continue to expand or coalesce to form a large-scale main crack. In the third stage, the large-scale crack causes a strength reduction of the baseplate fracture zone. The fracture zone experiences plastic deformation with obvious dimple and tearing features. Finally, the stress exceeds the ultimate strength of the baseplate material, causing rapid fracture. This is the mechanism behind the fatigue failure of the vibrator.

5. Analysis of the fatigue life of the baseplate specimen

We have developed an innovative approach to revolutionise the prediction of the fatigue life for baseplate specimens and enhance the reliability of fatigue-resistant designs. Our method deviates from the conventional cumulative damage method (S-N method) by incorporating an advanced parameter correction technique in conjunction with fatigue testing. Through the implementation of this cutting-edge approach, we have significantly improved the accuracy and efficiency of baseplate fatigue life forecasting. Furthermore, this innovative breakthrough minimises the risk of fatigue failure and substantially reduces reliance on traditional fatigue tests, thus streamlining the design process. The S-N curve fitting process is shown in Fig. 20.

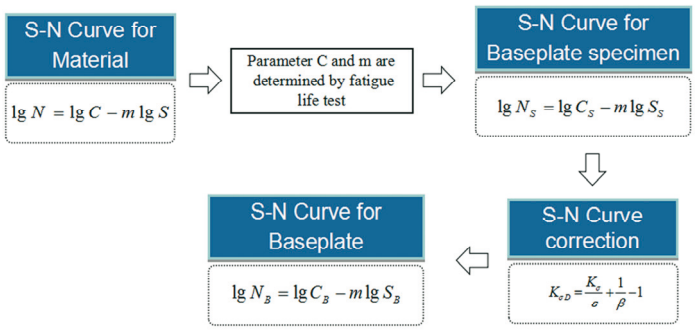

Fig. 20 S-N curve fitting process

(1) Experimental analysis of the baseplate fatigue life

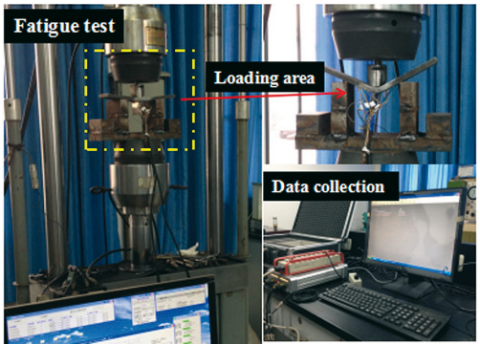

Fig. 21 MTS-810 Fatigue testing machine

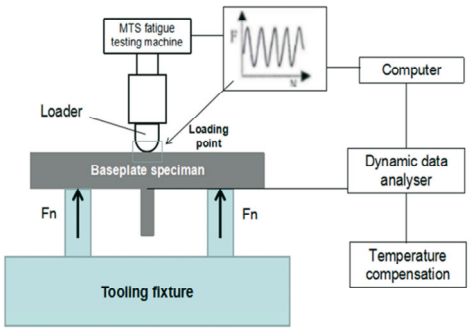

Fig. 22 The schematic diagram of the three-point bending fatigue test

The three-point bending method was used to test the baseplate specimen fatigue life. The material under the test was placed on the support points and then a force was applied at the loading point in the centre of the material to produce bending deformation (Figs. 21 and 22). The loading amplitude was 36 kN and the loading frequency was 8-12 Hz. A sampling rate of 10-20 kHz was used during loading to observe crack growth in the weld toe and substrate. The crack length was measured by the DIC technique. When all three types of specimens (Figs. 23, 24 and 25) were fractured, the sizes of the cracks and number of cycles to fracture for the weld toe and substrate failures were obtained. The results are shown in Table 3.

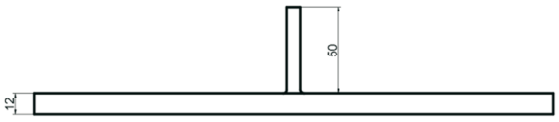

Fig. 23 Specimen I

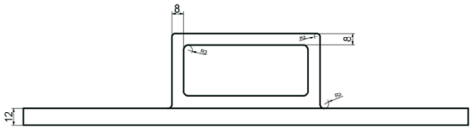

Fig. 24 Specimen II

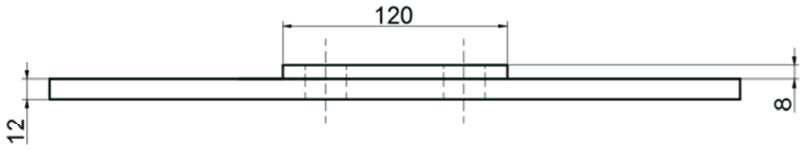

Fig. 25 Specimen III

The formula for the fatigue crack expanded life of a critical structure is given by:

$$N_f = \frac{(1-R)K_C}{C(Y_S\Delta\sigma\sqrt{\pi})^{\mathrm{m}}(0.5m-1)}\left(\frac{1}{a_0^{0.5m-1}}-\frac{1}{a_c^{0.5m-1}}\right)-\frac{1}{C(Y_S\Delta\sigma\sqrt{\pi})^{\mathrm{m\text{-}1}}(0.5m-1.5)}\left(\frac{1}{a_0^{0.5m-1.5}}-\frac{1}{a_c^{0.5m-1.5}}\right)$$
$$=\frac{1.09976\times10^{13}(1-R)}{(\Delta\sigma)^{3.5}}\left(\frac{1}{a_0^{0.75}}-\frac{1}{a_c^{0.75}}\right)-\frac{0.1166\times10^{13}}{(\Delta\sigma)^{2.5}}\left(\frac{1}{a_0^{0.25}}-\frac{1}{a_c^{0.25}}\right) \quad (23)$$

a_0 Initial crack size,
a_c Critical crack size,
C, m Material constants (obtained from experiments),
R Stress ratio,
$\Delta\sigma$ Stress range,
K_c Material fracture toughness,
Y_s Magnification factors of the stress intensity factor.

Table 2 Fracture mechanical parameters of specimens

number	C	m	a_0 (mm)	a_c (mm)	Y_S	R	K_C
I1	8.2×10^{-13}	3.5	0.5	11	1	0.794	50.14
I2				10.5			
I3				9.5			
II1				10.5	1.1		
II2				10			
II3				9			
III1				11	1.16		
III2				10			
III3				11			

Table 3 Crack length and fatigue life for the three specimen types

category	number	Crack size on welding consumables (mm)	Crack size in the direction of the substrate (mm)	Final number of cycles (cycles)	Average life (cycles)	Life expectancy from the fracture mechanics method (cycles)
I	I1	73	11	6.244×10^5	5.815×10^5	6.053×10^5
	I2	63	10.5	5.8×10^5		6.009×10^5
	I3	69	9.5	5.4×10^5		6.075×10^5
II	II1	61	10.5	3.376×10^5	3.196×10^5	2.983×10^5
	II2	59	10	3.192×10^5		2.922×10^5
	II3	55	9	3.02×10^5		2.952×10^5
III	III1	51	11	1.854×10^5	1.718×10^5	1.615×10^5
	III2	42	10	1.573×10^5		1.682×10^5
	III3	46	11	1.726×10^5		1.753×10^5

(2) Test fitting of the S-N curve of the plate specimen

The S-N curve of the plate specimen can be obtained by fitting the fatigue life test data of the plate at a certain stress level. The logarithmic relationship is:

$$\lg N_S = \lg C_S - m \lg S_S \tag{24}$$

It can be seen that lg N_S and lg S_S form a linear relationship, where both C and m are constants. For grade 45 steel under normal temperature conditions, the parameter m=7.3144 is determined from the metal fatigue test specification and structural steel material parameter selection [32]. According to the fatigue test life data of the three types of specimens and the corresponding stress level, the size of parameter C can be determined according to the linear relationship (Table 4).

Table 4 Statistical table of the S-N curve parameters for the three test pieces

Specimen category	Specimen number	Life N (Cycles) test value	S (Mpa)	lg N_S	lg S_S	lg C_S	Data function
Class I	I1	6.244×10^5	270	5.7955	2.4314	23.5797	Fit
	I2	5.8×10^5	275	5.7634	2.4393	23.6054	Fit
	I3	5.4×10^5	278	5.7324	2.4440	23.6088	Check
Class II	II1	3.376×10^5	295	5.5284	2.4698	23.5935	Fit
	II2	3.192×10^5	297	5.5041	2.4728	23.5911	Fit
	II3	3.02×10^5	300	5.4800	2.4771	23.5985	Check
Class III	III1	1.854×10^5	320	5.2681	2.5051	23.5914	Fit
	III2	1.573×10^5	328	5.1967	2.5159	23.5989	Fit
	III3	1.726×10^5	322	5.2370	2.5079	23.5807	Check

Therefore, the logarithmic S-N curve for the three kinds of specimens is:

$$\lg N_S = \lg C_S - 7.3144 \lg S_S \tag{25}$$

The mean values of the parameters for the three types of test pieces are calculated from the first two test datasets for each type of test piece using the fitting data from Eq. (26), as shown in Table 5.

Table 5 S-N curve parameters mean values for the three types of test pieces

Specimen category	Life mean N (Cycles)	S (MPa) mean	lg N_S mean	lg S_S mean	lg C_S mean
Class I	6.022×10^5	272.5	5.7794	2.43535	23.5925
Class II	3.284×10^5	276	5.5162	2.4713	23.5923
Class III	1.7135×10^5	324	5.2324	2.5105	23.5951
The mean fitting result of lg C_S		23.5933			

Under the tested conditions, the logarithmic form of the plate specimen S-N curve calculated by Table 4 is expressed as (Fig. 26):

$$\lg N_S = 23.5933 - 7.3144 \lg S_S \tag{26}$$

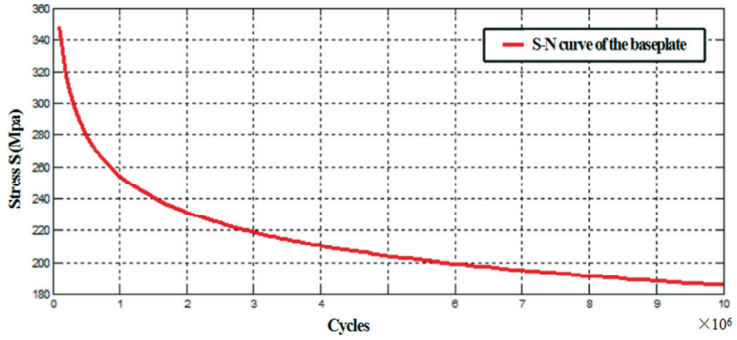

Fig. 26 S-N curve of the plate specimen

(3) The S-N curve for the plate structure

Once the scale plate specimen S-N curve is experimentally obtained, the specimen's S-N curve cannot be directly used for the prediction of plate life because of the differences in the structural size, stress state, surface roughness, and other factors compared to the full-scale plate

component. In addition, the S-N curve for the full-scale plate component is usually difficult to obtain using test methods [33]. The component S-N curve is corrected by the S-N curve of the material or specimen, as shown in Eqs. (28) and (29):

$$N = c\sigma_{-1}^{-m} \tag{27}$$

$$N = c(K_{\sigma D} \cdot \sigma_{-1D})^{-m} \tag{28}$$

Among them, $K_{\sigma D} = \frac{K_\sigma}{\varepsilon} + \frac{1}{\beta} - 1$.

Converting Eq. (29) into the logarithmic form, we arrive at:

$$\lg N = \lg c - m \lg \sigma_{-1D} - m \lg K_{\sigma D} \tag{29}$$

Equation (28) describes the S-N curve for the baseplate material, and Eq. (29) defines the S-N curve for the baseplate component. Among these, σ_{-1} is the symmetrical cyclic stress amplitude of the material or specimen, σ_{-1D} is the symmetrical cyclic stress amplitude of the component, c and m are material constants, $K_{\sigma D}$ is the correction coefficient, K_σ is the effective stress concentration factor, ε is the size coefficient, and β is the coefficient of the surface state, as shown in Table 6.

Table 6 Correction parameters

Parameters	Value	Statement
Size coefficient ε	0.882	Anti-fatigue design
Coefficient of surface state β	1	The surface of the flat adopts the grinding process
Effective stress concentration factor Kσ	1.175	The method for determining the stress concentration factor of materials in Zhao Shaobian in the literature

Thus, $K_{\sigma D}$ is calculated using the following formula:

$$K_{\sigma D} = \frac{K_\sigma}{\varepsilon} + \frac{1}{\beta} - 1 \tag{30}$$

In the previous section, the S-N curve was fitted by the plate specimen fatigue test as follows:

$$\lg N = 23.5933 - 7.3144 \lg S \tag{31}$$

Thus, the modified plate S-N curve is determined according to Eq. (30) and is shown in Fig. 27:

$$\lg N = 22.6826 - 7.3144 \lg S \tag{32}$$

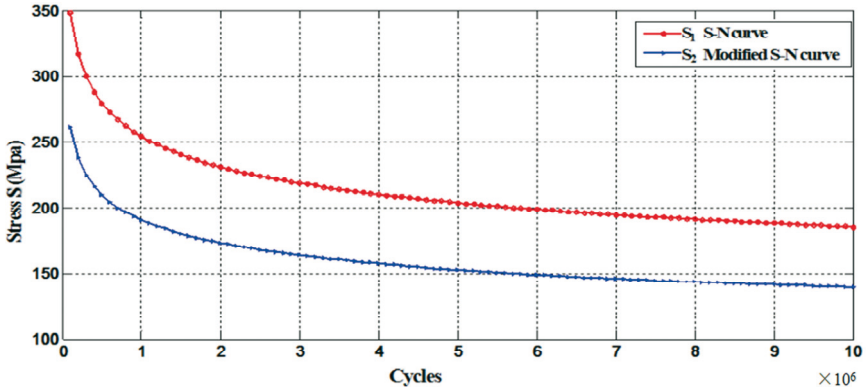

Fig. 27 S-N curve before and after the plate correction

(4) Comparative analysis of life prediction

According to the life prediction formula, the baseplate service life is closely related to the stress response. The vibrator baseplate's life is calculated in Table 7.

Table 7 Comparison of the theoretical and experimental fatigue lives of the baseplate

Number	I1	I2	I3	II1	II2	II3	III1	III2	III3	Average
Testing life	6.244 $\times10^5$	5.8 $\times10^5$	5.4 $\times10^5$	3.376 $\times10^5$	3.192 $\times10^5$	3.02 $\times10^5$	1.854 $\times10^5$	1.573 $\times10^5$	1.726 $\times10^5$	3.576 $\times10^5$
S-N curve method	6.4466× 10^5	5.6370× 10^5	5.2069× 10^5	3.3731× 10^5	3.2105× 10^5	2.9829× 10^5	1.8605× 10^5	1.5531× 10^5	1.7776× 10^5	3.5609 $\times10^5$
Error (%)	3.24	-2.81	-3.57	-0.086	0.579	-1.228	0.351	-1.265	2.989	1.791
Mean square value	0.11×10^5									
Fracture mechanics method	6.053 $\times10^5$	6.009 $\times10^5$	6.075 $\times10^5$	2.983 $\times10^5$	2.922 $\times10^5$	2.952 $\times10^5$	1.615 $\times10^5$	1.682 $\times10^5$	1.753 $\times10^5$	3.5604 $\times10^5$
Error (%)	-3.06	3.6	12.5	-11.6	-8.45	-2.25	-12.9	6.93	1.56	6.983
Mean square value	0.305×10^5									

To compare the experimental test value and theoretical prediction value intuitively, the test fatigue life and theoretical prediction life are plotted using a histogram, as shown in Fig. 28.

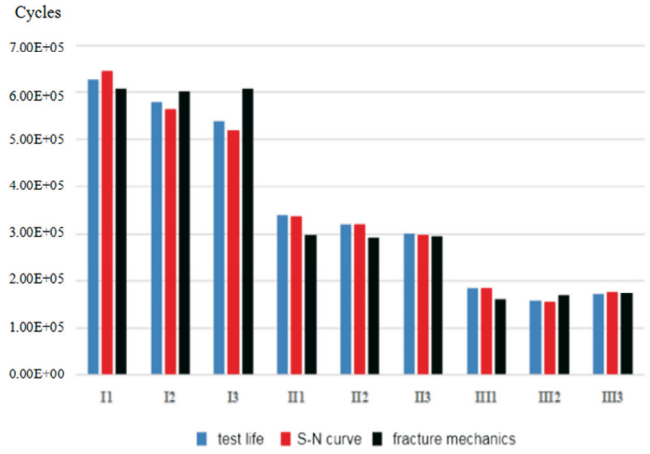

Fig. 28 Test and theoretical lives of the three types of specimens via a histogram comparative analysis

According to a comparison of the testing fatigue life and the theoretical calculation life for the three specimens, the results show that:

1) The testing fatigue lives and the two theoretical values of the nine test specimens are very close. Among them, the average error when using the S-N curve is 1.791%, and the average error for the fracture mechanics method is 6.983%, which are both within a reasonable range. In contrast, the S-N curve method has a relatively small error, and the accuracy is higher than when using the fracture mechanics method.

2) The average lives calculated by the S-N curve method and the fracture mechanics method are 3.5609×10^5 and 3.5604×10^5, respectively, which are all less than the test life. Among these, the error from the S-N curve is mainly associated with the deviation of the S-N curve. The error in the fracture mechanics method is due to the difficulty when considering the weld crack length, which leads to a slightly smaller estimate.

3) The mean value of the fatigue life reflects the deviation between the theoretical life calculated and the test life. In a comparative analysis, the S-N curve fatigue life average variance (0.11×10^5) is less than that from the fracture mechanics method (0.305×10^5). The S-N curve deviation is slightly smaller. A further comparison of the average fatigue life calculated from the two theoretical models shows that the average life calculated by the S-N curve and fracture mechanics methods is similar, indicating that the accuracy of the S-N method is slightly higher. However, the calculation accuracies of the two fatigue life theoretical models are similar.

6. Conclusions

(1) The loading cases for the vibroseis baseplate were determined by a vibration system dynamics analysis. The reaction force of the baseplate changed with time periodically and increased with the vibration displacement and frequency. Additionally, the joint between the baseplate and piston rod exhibited maximum deformation and damage, which enhanced the randomness of the fatigue crack growth, propagation speed, and fracture failure.

(2) Via the macroscopic and microscopic topography analysis of the baseplate fracture, the damage mechanism for the baseplate under the vibration conditions is described as having three stages: fatigue crack initiation (Stage I); fatigue crack propagation (Stage II); and fracture failure (Stage III). Fatigue cracks originate from defects in the baseplate welding parts. Micro voids and grooves caused by grain sliding under alternating stress serve as initiation sites for the micro-cracks. The micro-cracks propagate along the 0° and 45° directions, accompanied by transgranular and intergranular fracture. Finally, fracture occurs at the weakest parts, resulting in the instability and rapid fracture of the baseplate structure. This process is the mechanism underlying the fatigue failure of the vibrator.

(3) The fatigue life test is applied to fit the S-N curve of the baseplate. This method has the advantages of high efficiency and accuracy. It also has certain accuracy in predicting the fatigue life of mechanical structures under other complex working conditions. This method can be used for the fatigue life prediction of mechanical structures under complex loads with high accuracy and efficiency.

(4) The fatigue life analyses for the baseplate specimens using the S-N curve and fracture mechanics methods have slightly different accuracy. The fatigue lives calculated from the two theoretical methods were shorter than the test measured life value, and the accuracy of the fatigue life calculated by the S-N curve method was slightly higher than the fracture mechanics method. The accuracy of the S-N curve method depended highly on the accuracy of the S-N curve for the structural material. The calculation accuracy of the fracture mechanics method depended more on the selection of the crack propagation parameters for the structural material. These were the main sources of error for the two models.

Acknowledgments

This research received financial support from the open fund project of the SINOPEC Key Laboratory of Seismic Elastic Wave Technology [Research on the coupled vibration model of the vibroseis vibrator-earth and wave field dynamics] (33550000-22-ZC0613-0288). It was also supported by the Shale Gas Evaluation and Exploitation Key Laboratory of Sichuan Province (YSK2022013). This project was also funded by the Sichuan Science and Technology Program (grant no. 24NSFSC0551).

REFERENCES

[1] J. J. Xiong, Z. T. Gao, “Actual load spectrum data treatment system,” Journal of Beijing University of Aeronautics and Astronautics, vol. 22 no.4 pp. 438-441, 1996.

[2] D. B. Kececioglu, “Reliability Engineering Handbook (Volume 1) Endlewood Cliffs,” Prentice Hall Inc, 1996.

[3] K. Ni, Z. T. Ga, “Two Dimensional Probabilistic Miner Criterion for Fatigue reliability,” STRUCTURAL SAFETY AND RELIABILITY, vol.17 no.4 pp. 365-376, 2001, https://doi.org/10.19636/j.cnki.cjsm42-1250/o3.1996.04.014

[4] Z. X. Su. “Fatigue Life and Reliability Evaluation of Structures Subjected to Random Stress,” Journal of Mechanical Strength, vol. 21 no. 2 pp.137-141, 1999, https://doi.org/10.16579/j.issn.1001.9669.1999.02.016

[5] Y. Gu, “Damage Cumulative Model for the Fatigue Reliability Evaluation of Structural Element,” Journal of Mechanical Strength, vol.22 no.3, pp. 228-230, 2000, https://doi.org/10.16579/j.issn.1001.9669.2000.03.020

[6] Q. H. Wang, “Wind Fatigue Life Reliability Analysis for Structural System,” CHINA CIVIL ENGINEERING JOURNAL, vol.44, no.8, pp. 72-79, 2011, https://doi.org/10.15951/j.tmgcxb.2011.08.019

[7] Paris P C, Erdogan F. “A critical analysis of crack propagation laws. Journal of Basic Engineering,” ASME, vol.85, no.4, pp. 528-534, 1963, https://doi.org/10.1115/1.3656903

[8] Griffith AA. “The phenomena of rupture and flow in solids,” Philosophical Transactions of the Royal Society of London, vol.221, no.582-593, pp. 163-198, 1920, https://doi.org/10.1098/rsta.1921.0006

[9] J.A. Bea. “Corrections to B-models for fatigue life prediction of metals during crack propagation,” Numerical Methods in Engineering, vol.46, no.9, pp. 1405-1420, 1999, https://doi.org/10.1002/(SICI)1097-0207(19991130)46:9<1405::AID-NME705>3.0.CO;2-I

[10] C. Y. Shi. “Fatigue residual life reliability and sensitivity analysis for the Bridge Crane Metal Structure,” Taiyuan: Taiyuan University of Science and Technology, 2014.

[11] X. Y. Wang, “Estimate the Fatigue Life of Welded Hollow Spherical Joints in Grid Structure Based on Fracture Mechanics,” Taiyuan: Taiyuan institute of technology, 2010.

[12] B. Alfredsson. “Propagation of physically short cracks in a bainitic high strength bearing steel due to fatigue load,” International Journal of Fatigue, vol.90, no.2, pp.166–180, 2016, https://doi.org/10.1016/j.ijfatigue.2016.04.031

[13] X. M. Tan, “Fatigue life reliability evaluation method of aluminum alloy based on the fatigue crack initiation mechanism,” Journal of Aeronautics materials, vol.34, no.2, pp. 84-89, 2014.

[14] Dallas James Marein. “T-bar baseplate for a seismic signal transducer.” US4116299, 1978.

[15] Z. Chen, Z. Q. Huang, “The Fatigue Behavior and Fatigue Reliability Analysis of Vibroseis Baseplates Based on Fracture Mechanics,” PROCEEDINGS OF THE INSTITUTION OF MECHANICAL ENGINEERS PART O-JOURNAL OF RISK AND RELIABILITY, vol.231 no.6 pp.732-749, 2017, https://doi.org/10.1177/1748006X17731902

[16] J. J, Sallas. “Seismic Vibrator Control and the Down Going P-wave,” Geophysical Prospecting, vol.49, no.6, pp.732, 2006, https://doi.org/10.1190/1.1441701

[17] Robert Ley, Willem Adolfs, Ralph Bridle, Mohammad AL-Homaili, Aldo Vesnaver and Paul Ras. “Ground viscosity and stiffness measurements for near surface seismic velocity,” Geophysical Prospecting, vol.54, no.6, pp. 751-762, 2006, https://doi.org/ 10.1111/j.1365-2478.2006.00574.x

[18] X. Peng, L, Hao, “Numerical simulation of transverse wave controlled source vibrator-earth coupled vibration,” Petroleum Geophysical Exploration, vol. 58, no. 6, pp. 1349-1358, 2012, https://doi.org/10.13810/j.cnki.issn.1000-7210.2023.06.004

[19] J. Zhuang, “Amplitude-frequency Characteristics Analysis of the coupling vibration between the High Frequency Vibroseis and Earth,” Journal of Changchun University of Science and Technology, vol. 29, no. 2, pp. 184-187, 1999, https://doi.org/10.13278/j.cnki.jjuese.1999.02.020

[20] J. Xu, “Research of the Vibroseis Baseplate and Earth Vibration Model and Parameters,” Coal Geology of China, no. 3, pp. 62-64, 2001.

[21] J. G. Hu, “Dynamic Finite Element Analysis of the Vibroseis Baseplate,” Xian: Xian University of Technology, 2009.

[22] C. Wang, “Utility trench backfill compaction using vibratory plate compactor versus excavator-mounted hydraulic plate compactor(Article),” Journal of Pipeline Systems Engineering and Practice, vol.8, no.4, pp. 04017021, 2005, https://doi.org/10.1061/(ASCE)PS.1949-1204.0000284

[23] K. Chen, “Dynamic Analysis and Research of the Impact Rammer,” Xi An: Xi An University of Architecture and Technology, 2012.

[24] A. Q. Xu, “Dynamic Modeling and Vibration analysis of Underground Vibrator,” Vibration And Shock, vpl.26, no. 7, pp. 93-96, 2007, https://doi.org/10.13465/j.cnki.jvs.2007.07.022

[25] Y. J. Gao, “Structural Design and Dynamic Simulation of a New Type of High Power Vibratory Flat Rammer,” Xi An: Changan University, 2005.

[26] L. L. He, “Dynamic Analysis of an Automatic Vibratory Rolling Compaction Mechanism,” Construction Machinery, 1998.

[27] H. Tao, “Dynamic Model Research, Simulation and Optimization Design of Vibratory Plate Compactor,” Coal Mine Machinery, vol. 27, no. 7, pp. 24-26, 2006, https://doi.org/10.13436/j.mkjx.2006.07.011

[28] Z. X. Zhan, “Vibratory compactor vibratory compaction adhesion performance research,” Journal of Shandong Jiaotong University, vol. 22, no. 1, pp. 82-86, 2014.

[29] H. Y. Xiao, J. Pan, “Vibration analysis of a cylinder with slight diameter and thickness variations,” Journal of Vibroengineering, vol.19, no. 2, pp.844-863, 2017, https://doi.org/10.21595/jve.2016.17610

[30] J. M. Pan. “Study on Fatigue Crack Propagation Law of Back Axle Using Real-time Monitoring of Strain,” Journal of Tongji University, no. 6, pp. 745-748, 1999.

[31] B. Y. Wang, “Study on Fatigue Fracture Mechanism and Preventive Measures of Oil Tank in Pumping Unit,” Hangzhou: Zhejiang University, 2002.

[32] Y. X . Zhao, “A Unified Approach to Probabilistic Design of S-N Curves for Three Commonly Used Stress Life Models,” Nuclear Power Engineering, vol.22, no.1, pp. 42-52, 2001.

[33] W. C. Cui, “A Preliminary Review of Recent Developments in Life Prediction Methods of Marine Structures,” Journal of Ship Mechanics, vol. 3, no. 6, pp.55-79, 1999.

Submitted: 05.9.2023

Accepted: 05.02.2024

Zhen Chen*
State Key Laboratory of Shale Oil and Gas Enrichment Mechanisms and Effective Development
Sinopec Key Laboratory of Seismic Elastic Wave Technology
Southwest Petroleum University, Chengdu, Sichuan, 610500, P.R. China
Chaocheng Wei
Shulong Nie
Oil and Gas Equipment Technology Sharing and Service Platform of Sichuan Province, Southwest Petroleum University, Chengdu, Sichuan, 610500, P.R. China
Ling Liu
Engineering and Technology Research Institute, of Western Drilling Engineering, CNPC
Shuang Jing
Zhiqiang Huang
Oil and Gas Equipment Technology Sharing and Service Platform of Sichuan Province, Southwest Petroleum University, Chengdu, Sichuan, 610500, P.R. China
Lei Hao
Bureau of Geophysical Prospecting International, CNPC, Zhuozhou, Hebei, China
Guangjing Zhou
Branch Technical Services Company, of Western Drilling Tubing & Well Control Technical Services, Chengdu, China
*Corresponding Author:
971857707@qq.com